Received: 16 January 2020

DOI: 10.1002/mma.6338

SPECIAL ISSUE PAPER

WILEY

Local thermal nonequilibrium conjugate natural convection of nano-encapsulated phase change particles in a partially porous enclosure

S. A. M. Mehryan[1] | **Muneer Ismael**[2] | **Mohammad Ghalambaz**[3,4]

[1]Young Researchers and Elite Club, Yasooj Branch, Islamic Azad University, Yasooj, Iran

[2]Mechanical Engineering Department, College of Engineering, University of Basrah, Basrah, Iraq

[3]Metamaterials for Mechanical, Biomechanical and Multiphysical Applications Research Group, Ton Duc Thang University, Ho Chi Minh City, Vietnam

[4]Faculty of Applied Sciences, Ton Duc Thang University, Ho Chi Minh City, Vietnam

Correspondence
Mohammad Ghalambaz, Ton Duc Thang University, Ho Chi Minh City, Vietnam.
Email: mohammad.ghalambaz@tdtu.edu.vn

This paper analyzes the heat transfer process of nano-encapsulated phase change material (NEPCM) particles suspended in a base fluid. NEPCMs are polyurethane-nonadecane, and the base fluid is water. The formed suspension fills a system of two different layers: a porous layer and a clear layer. A thermally conductive solid wall transmits heat to the porous layer. These three partitions are confined in a square cavity. The cavity is heated from the left side of the solid wall and cooled from the right side of the clear layer. The solid matrix of the porous layer and the suspension are in local thermal nonequilibrium. A Galerkin-weighted residual finite element method is adopted for numerical computations. The impacts of Stefan number, fusion temperature, and the nanoparticles volume fraction are inspected, graphically. Results show that the maximum heat transfer can be attained with lower Stefan number, higher nanoparticles volume fraction, and a fusion temperature range between 0.2 and 0.6. For a certain circumstance, it is found that enhancement of about 29% in heat transfer can be gained when the volume fraction of the NEPCM particles is raised from 0 to 0.05.

KEYWORDS

local thermal nonequilibrium (LTNE), nano-encapsulated phase changematerial (NEPCMs) particles, phase change materials (PCMs), porous layer, suspension of NEPCMs

1 | INTRODUCTION

The high thermal storage of phase change materials (PCMs) has qualified them to be a perfect choice for conserving energy. Due to their compliant phase change, PCMs absorb heat and release it with finite temperature differences; hence, they are active when a variation in environmental conditions exists. The concept of PCMs is increasingly developing to magnify the thermal mass (heat capacity) of building envelopes[1] and to provide efficient portable electronic devices.[2] For the sake of high-energy storage, the thermal conductivity of PCMs should be as high as possible. Thus, studies have focused to increase this physical property by dispersing solid nanoparticles having higher thermal conductivity.[3] When phase change occurs, the volume of PCMs varies and may need to be controlled; moreover, they may react with the outside environment.[4] To avoid these two drawbacks, the PCM is encapsulated in a shell material. The encapsulation not only prevents these two drawbacks but also increases the area of heat transfer. Consequently, the tri-concepts; nanoparticles-encapsulated-phase change material (NEPCMs) have become an excellent vehicle of investigation. Moreover, the simple[5–8] or hybrid[9, 10] nanofluids nanoparticles with no phase change have been extensively investigated in literature as additives for thermal enhancement. The

migration of nanoparticles in the free convection flows using Buongiorno's mathematical model is also investigated in Sheremet et al[11] and Revnic et al.[12] Menni et al[13–15] also reviewed the heat transfer enhancement of nanofluids in porous media,[13] complex geometries,[14] and solar collectors.[15]

Faden et al[16] developed a numerical algorithm to resolve the melting and settling of macro-EPCMs and got a stable solution. The developed new algorithm enabled a wide temperature range between the PCM and the wall of the studied cavity with no oscillated results. They conducted an experimental study to demonstrate their numerical findings and gave explanations to the discrepancies between the two results. Khodadadi and Hosseinizadeh[3] contributed to founding the pillars of nanoparticles enhanced PCMs, where they predicted a promising virtue of the thermal conductivity of the PCMs. Hosseinizadeh et al[17] widened the governing parameters to include Stefan number and endorsed the conclusion of Khodadadi and Hosseinizadeh,[3] where they performed a numerical study of unconstrained NEPCMs inside a circular enclosure. Their study was transient, and hence, they took into account the subcooled region. Ghalambaz et al[18] investigated the effect of using hybrid nanofluid in enhancing the melting process inside a square cavity. They found better fusion performance with the use of such hybrid nanoparticles.

Jourabian et al[19] used the lattice Boltzmann numerical method to study the transient melting of ice as a PCM enclosed by annulus with dispersing copper nanoparticles with different volume fractions. The improvement of thermal conductivity and the decrease of latent heat of fusion were the attributions of the expediting melting rate. Kashani et al[20] proposed that proper suspensions like Cu-n-hexadecane can appreciably improve the heat transfer and hence the solidification inside the square enclosure as thermal energy storage. Elbahjaoui and El Qarnia[21] considered a latent heat storage system composed of multi-slabs of PCMs between them a heat transfer fluid (water) flows. Due to symmetry, one-half of both PCM slab and water channels were computed. The PCM slab composed of Paraffin with alumina nanoparticles dispersed. The volume fraction of the alumina has considerably decreased the time required for complete melting.

In porous media, the solid/liquid phase change has received distinct concerns as it designates not only engineering applications but also some important geophysical applications such as artificial freezing of ground to support construction or mining and freezing of soil surrounding the pipes of underground heat exchangers.[22] The numerical and experimental results of Beckermann and Viskanta[23] put the basis of the shape influence of the solid/liquid interface by the natural convection and conduction in the liquid and solid phases, respectively. However, the numerical analysis was based on the macroscopic volume averaged over a porous medium element.

Trellers and Dufly[24] were interested in using the thermal energy storage system in thermoelectric cooling implemented in the vaccine refrigerator. Their problem, as such, was two containers: the inner one, which is filled with water and including vaccine and the outer is filled with PCM involved in aluminum porous-matrix and occupies the inner container. To avoid the need for interface boundary conditions, they followed the enthalpy method in which the solid-liquid mushy zone is dealt as a porous medium. A small temperature difference between the water and the PCM was assigned due to the existence of the aluminum porous medium where it improves the thermal conductivity and as a result, reduces the thermal resistance.

Regarding the thermodynamics action, considering local thermal equilibrium (LTE) between the solid matrix and the fluid is prone to erratic results, especially for high Reynolds and Darcy numbers.[25] When the thermal conductivity of the porous matrix is low and the interaction between the liquid and the porous structure is high, it can be assumed that the temperature of the porous matrix and the fluid inside the pores are identical. In this case, the LTE model with one heat equation can represent the thermal behavior of the porous matrix and the fluid inside the pores. Various aspect of heat transfer in a porous medium such as non-Darcy effects,[26] using nanofluids,[6] hybrid nanofluids with carbon nanotubes,[7,27] magnetic field effects, and [28] entropy generation[29] are investigated using LTE model in recent studies.

However, the LTE is also not valid when the thermal conductivities and heat capacities of the solid matrix and the liquid are notably different.[30] Therefore, it was asserted that the local thermal nonequilibrium (LTNE) is an essential treatment in backed-beds implemented in thermal energy storage.[25,31] Consequently, a significant difference between the distribution of temperatures in the liquid phase and the solid matrix was reported.[32]

In recent years, modeling with LTNE has been adopted widely even far from the latent heat storage system.[33–36] However, Harris et al[37] tried to approximate a procedure to analyze the conduction heat transfer in the solid matrix during the phase change by assuming LTNE. Relations describing the slow melting or freezing process have endorsed the invalidation of the thermal equilibrium assumption. Very recently, many aspects of heat transfer in porous cavities with no phase change such as heating boundary conditions,[36] conjugate heat transfer,[38] and hybrid nanofluids[35] are addressed using the LTNE model.

The phase change thermal energy storage and heat transfer of a suspension containing NEPCMs is a new subject in natural convection flows. The nano-encapsulated particles are made of a nano-phase change core and a shell as the encapsulation material. The NEPCM nanoparticles undergo a phase change in the suspension, and they can transfer energy in the form of latent heat. In a pioneer study, Ghalambaz et al[39] investigated the steady-state natural convection phase change of a dilute suspension compromising n-octadecane nanoparticles encapsulated in a tiny shell of poly-methyl methacrylate and dispersed in water. The suspension is enclosed by a square cavity and subjected to natural convection. Despite the general enhancement of heat transfer gained by the nanoparticle dispersion, some adverse actions were recorded, such as weakening of the buoyancy force. The study remarked that the fusion temperature was the key parameter that governs the melting of the NEPCMs. Following,[39] Hajjar et al[40] addressed the unsteady heat transfer of a NEPCM-suspension in a cavity. Considering the natural convection of NEPCMs in porous media, in a very recent study, Ghalambaz et al[41] explored the mixing convection heat transfer of NEPCMs in the boundary layer over a hot vertical plate embedded in a porous medium. The results show that there are two solution branches for flow and heat transfer over the plate, which only one of the solution branches is stable. Moreover, the authors reported that the presence of encapsulated phase change nanoparticles enhances the heat transfer rate. The lower the fusion temperature of the nanoparticle's phase-change core, the better the heat transfer rate.

In another recent study, Ghalambaz et al[42] investigated the unsteady free convection heat transfer of a NEPCMs suspension in a cavity. The porous matrix was made of glass balls, and a NEPCM-water suspension saturated the porous pores. The phase change core of the nanoparticles was nonadecane, and polyurethane (PU) was used as the shell material to enclose the phase change core. Because of the low thermal conductivity of the glass-ball porous matrix, the simple LTE approach was employed. The results reveal that the presence of NEPCM particles enhances the heat transfer and the increase of volume fraction of the nanoparticles improves the Nusselt number. The increase of the porosity raises the heat transfer rate only when the volume fraction of nanoparticles is higher than 3%; otherwise, the increase of porosity reduces the heat transfer rate. An optimum fusion range was also observed for heat transfer enhancement. Hence, the volume fractions of nanoparticles (NEPCMs particles) and their fusion temperature are two major parameters for heat transfer enhancement of using NEPCMs particles in natural convection flows. It should be noted that the study of Ghalambaz et al[42] is limited to the LTE model, which is applicable for the porous matrixes with low thermal conductivities and low fluid motion in porous pores. However, there are many applications, in which, a layer of metal foam with high thermal conductivity can be employed to improve the heat transfer rate. Such a metal foam layer can be also used as a charging layer to heat the NEPCM-suspension and store latent thermal energy in the nanoparticles core.

The encapsulation of PCMs is promising for enhancing the heat transfer along with thermal energy storage. Hence, following the work of Ghalambaz et al,[42] the present study aims to address the heattransfer of the NEPCM-suspensions in a layer of the porous medium using the LTNE model for the first time.

2 | MATHEMATICAL FORMULATION

An incompressible and laminar flow arising from the natural convection of a suspension inside a partially layered cavity is numerically analyzed. As demonstrated in Figure 1, a heat-conducting wall having the-width d is connected to the left hot wall. A porous layer of width s is placed in contact with the conducting wall. The other layer, that is, a clear layer, is in the vicinity of the cold wall. The suspension is a mixture of water and nano-encapsulated particles of a phase change substance. The materials of the shell and core of the particles are polyurethane (PU) and nonadecane, respectively, and their thermophysical properties are inserted in Table 1.

The PCM core absorbs some heat and undergoes a phase change when its temperature reaches the fusion temperature. The Boussinesq approximation is adopted to model the effects of gravity force. A LTNE is considered between the solid and fluid structures of the porous region. The flow hydrodynamic in the porous layer can be depictured by applying the Brinkman-extended Darcy mathematical model. Thus, under these assumptions, the conservation equations for the different layers can be represented as follows:

1. Clear layer:

$$\frac{\partial u}{\partial x}+\frac{\partial v}{\partial y}=0, \tag{1}$$

$$\rho_{nf}\left(u\frac{\partial u}{\partial x}+v\frac{\partial u}{\partial y}\right)=-\frac{\partial p}{\partial x}+\mu_{nf}\left(\frac{\partial^2 u}{\partial x^2}+\frac{\partial^2 u}{\partial y^2}\right), \tag{2}$$

$$\rho_{nf}\left(u\frac{\partial v}{\partial x}+v\frac{\partial v}{\partial y}\right)=-\frac{\partial p}{\partial y}+\mu_{nf}\left(\frac{\partial^2 v}{\partial x^2}+\frac{\partial^2 v}{\partial y^2}\right)+g\rho_{nf}\beta_{nf}\left(T_{nf}-T_c\right), \tag{3}$$

$$\left(\rho C_p\right)_{nf}\left(u\frac{\partial T_{nf}}{\partial x}+v\frac{\partial T_{nf}}{\partial y}\right)=k_{nf}\left(\frac{\partial^2 T_{nf}}{\partial x^2}+\frac{\partial^2 T_{nf}}{\partial y^2}\right). \tag{4}$$

2. Porous layer:

$$\frac{\partial u}{\partial x}+\frac{\partial v}{\partial y}=0, \tag{5}$$

$$\frac{\rho_{nf}}{\varepsilon^2}\left(u\frac{\partial u}{\partial x}+v\frac{\partial u}{\partial y}\right)=-\frac{\partial p}{\partial x}+\frac{\mu_{nf}}{\varepsilon}\left(\frac{\partial^2 u}{\partial x^2}+\frac{\partial^2 u}{\partial y^2}\right)-\frac{\mu_{nf}}{K}u, \tag{6}$$

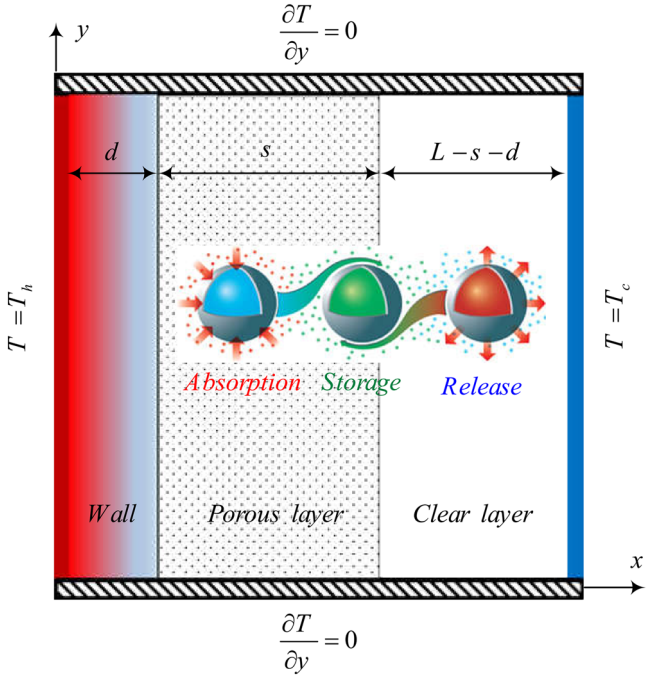

FIGURE 1 Schematic view of the studied geometry [Colour figure can be viewed at wileyonlinelibrary.com]

TABLE 1 Thermophysical properties of the host fluid, the core (nonadecane), and the shell (PU)[59,60]

	μ (kg m^{-1} s^{-1})	β (K^{-1})	k (Wm^{-1} K^{-1})	C_p (kJ kg^{-1} K^{-1})	ρ (kgm^{-3})
Host fluid	8.9×10^{-4}	21×10^{-5}	0.613	4179	997.1
Nonadecane	—	—	—	2037	721
PU	—	17.28×10^{-5}	—	1317.7	786

Abbreviation: PU, polyurethane.

$$\frac{\rho_{nf}}{\varepsilon^2}\left(u\frac{\partial v}{\partial x}+v\frac{\partial v}{\partial y}\right)=-\frac{\partial p}{\partial y}+\frac{\mu_{nf}}{\varepsilon}\left(\frac{\partial^2 v}{\partial x^2}+\frac{\partial^2 v}{\partial y^2}\right)+g\rho_{nf}\beta_{nf}\left(T_{nf}-T_c\right)-\frac{\mu_{nf}}{K}v, \tag{7}$$

$$\left(\rho C_p\right)_{nf}\left(u\frac{\partial T_{nf}}{\partial x}+v\frac{\partial T_{nf}}{\partial y}\right)=\varepsilon k_{nf}\left(\frac{\partial^2 T_{nf}}{\partial x^2}+\frac{\partial^2 T_{nf}}{\partial y^2}\right)+h\left(T_s-T_{nf}\right), \tag{8}$$

$$0=(1-\varepsilon)k_s\left(\frac{\partial^2 T_s}{\partial x^2}+\frac{\partial^2 T_s}{\partial y^2}\right)-h\left(T_s-T_{nf}\right). \tag{9}$$

3. Thick wall:

$$k_w\left(\frac{\partial^2 T_w}{\partial x^2}+\frac{\partial^2 T_w}{\partial y^2}\right)=0. \tag{10}$$

2.1 | Boundary and interface conditions

It is considered that the continuities of the velocity and temperature at the interface of the porous and clear layers are established. The temperature continuity can be acceptable when the heat transfer at the interface is large enough.[43–47]

$$\begin{aligned} &v_{CL}=v_{PL}, u_{CL}=u_{PL}, \mu_{nf}\frac{\partial u}{\partial n}\bigg|_{CL}=\mu_{nf,eff}\frac{\partial u}{\partial n}\bigg|_{PL}, \mu_{nf}\frac{\partial v}{\partial n}\bigg|_{CL}=\mu_{nf,eff}\frac{\partial v}{\partial n}\bigg|_{PL}\\ &T_{nf}\big|_{CL}=T_{nf}\big|_{PL}=T_s|_{PL}, k_{nf}\frac{\partial T_{nf}}{\partial n}\bigg|_{CL}=k_{nf,eff}\frac{\partial T_{nf}}{\partial n}\bigg|_{PL}+k_{s,eff}\frac{\partial T_s}{\partial n}\bigg|_{PL}=q_i'', \end{aligned} \tag{11}$$

in which

$$\mu_{nf,eff}=\frac{\mu_{nf}}{\varepsilon}, k_{nf,eff}=\varepsilon k_{nf}, k_{s,eff}=(1-\varepsilon)k_s. \tag{12}$$

Considering no-temperature-jump condition on the walls and the energy balance on the wall-porous interface, the thermal conditions are

$$\begin{aligned} &T_w|_{wall}=T_{nf}\big|_{PL}=T_s|_{PL}\\ &k_w\frac{\partial T_w}{\partial n}\bigg|_{wall}=k_{nf,eff}\frac{\partial T_{nf}}{\partial n}\bigg|_{PL}+k_{s,eff}\frac{\partial T_s}{\partial n}\bigg|_{PL}=q_i''. \end{aligned} \tag{13}$$

In addition, the left of the conducting wall and the right of the clear layer are at the higher and lower temperatures. By considering the no-slip condition of the viscous suspension, the velocity on the walls is equal to zero.

$$\begin{aligned} &v(x,0)=u(x,0)=0, \frac{\partial T_w(x,0)}{\partial y}=\frac{\partial T_{nf}(x,0)}{\partial y}=\frac{\partial T_s(x,0)}{\partial y}=0\\ &v(x,L)=u(x,L)=0, \frac{\partial T_w(x,L)}{\partial y}=\frac{\partial T_{nf}(x,L)}{\partial y}=\frac{\partial T_s(x,L)}{\partial y}=0\\ &v(L,y)=u(L,y)=0, T_{nf}(L,y)=T_c, T_w(0,y)=T_h \end{aligned} \tag{14}$$

2.2 | Suspension bulk properties

The following weighted function is employed to achieve the density of the suspension[48]:

$$\rho_{nf} = (1-\phi)\rho_{bf} + \phi\rho_p, \tag{15}$$

in which the density of NEPCM particles is[49]

$$\rho_p = \frac{(1+\iota)\rho_{co}\rho_{sh}}{\rho_{sh} + \iota\rho_{co}}, \tag{16}$$

To evaluate the specific heat capacity of the suspension, the following relation is utilized[49,50]:

$$C_{p,nf} = \frac{(1-\phi)(\rho C_p)_{bf} + \phi(\rho C_p)_p}{\rho_{nf}}. \tag{17}$$

The suspension's coefficient of the thermal expansion is defined using the following linear relation[50]:

$$\beta_{nf} = (1-\phi)\beta_{bf} + \phi\beta_p. \tag{18}$$

Since the PCM as the core of nanoparticles can be melted, it can absorb a large amount of heat. Hence, the specific heat capacity of the particles must also include the latent heat of the PCM[48,51]:

$$\begin{aligned} C_{p,p} &= C_{p,p} + \left\{\frac{\pi}{2}\cdot\left(\frac{h_{sf}}{T_{Mr}} - C_{p,co}\right)\cdot\sin\left(\pi\frac{T-T_0}{T_{Mr}}\right)\right\}\sigma \\ \sigma &= \begin{cases} 0 & T < T_0 \\ 1 & T_0 < T < T_1 \\ 0 & T > T_1 \end{cases} \Bigg| \begin{cases} T_0 = T_{fu} - T_{Mr}/2 \\ T_1 = T_{fu} + T_{Mr}/2 \end{cases}. \end{aligned} \tag{19}$$

The below linear relations are applied to calculate the thermal conductivity and dynamic viscosity of the NEPCM-suspension, consisting of nano-encapsulated particles[52,53]:

$$\frac{k_{nf}}{k_{bf}} = 1 + Nc\phi, \tag{20a}$$

$$\frac{\mu_{nf}}{\mu_{bf}} = 1 + Nv\phi. \tag{20b}$$

2.3 | Dimensionless equations

Using the nondimensional parameters,

$$\begin{aligned} &X = \frac{x}{L},\ Y = \frac{y}{L},\ D = \frac{d}{L},\ S = \frac{s}{L}, U = \frac{uL}{\alpha_{bf}},\ V = \frac{vL}{\alpha_{bf}} \\ &P = \frac{pL^2}{\rho_{bf}\alpha_{bf}^2}, \theta_{nf} = \frac{T_{nf}-T_c}{\Delta T}, \theta_s = \frac{T_s-T_c}{\Delta T}, \theta_w = \frac{T_w-T_c}{\Delta T}, \end{aligned} \tag{21}$$

in which $\Delta T = T_h - T_c$, the conservation equations, interface, and boundary conditions are transferred to dimensionless coordinate as:

1. Clear layer:

$$\frac{\partial U}{\partial X} + \frac{\partial V}{\partial Y} = 0, \tag{22}$$

$$\left(\frac{\rho_{nf}}{\rho_{bf}}\right)\left(U\frac{\partial U}{\partial X} + V\frac{\partial U}{\partial Y}\right) = -\frac{\partial P}{\partial X} + Pr(1+Nv\phi)\left(\frac{\partial^2 U}{\partial X^2} + \frac{\partial^2 U}{\partial Y^2}\right), \tag{23}$$

$$\begin{aligned}\left(\frac{\rho_{nf}}{\rho_{bf}}\right)\left(U\frac{\partial V}{\partial X} + V\frac{\partial V}{\partial Y}\right) &= -\frac{\partial P}{\partial Y} + Pr(1+Nv\phi)\left(\frac{\partial^2 V}{\partial X^2} + \frac{\partial^2 V}{\partial Y^2}\right)\\ &+ Ra{\cdot}Pr\left(\frac{\beta_{nf}}{\beta_{bf}}\right)\left(\frac{\rho_{nf}}{\rho_{bf}}\right)\theta_{nf},\end{aligned} \tag{24}$$

$$Cr\left(U\frac{\partial \theta_{nf}}{\partial X} + V\frac{\partial \theta_{nf}}{\partial Y}\right) = (1+Nc\phi)\left(\frac{\partial^2 \theta_{nf}}{\partial X^2} + \frac{\partial^2 \theta_{nf}}{\partial Y^2}\right). \tag{25}$$

2. Porous layer:

$$\frac{\partial U}{\partial X} + \frac{\partial V}{\partial Y} = 0, \tag{26}$$

$$\varepsilon^{-2}\left(\frac{\rho_{nf}}{\rho_{bf}}\right)\left(U\frac{\partial U}{\partial X} + V\frac{\partial U}{\partial Y}\right) = -\frac{\partial P}{\partial X} + Pr\varepsilon^{-1}(1+Nv\phi)\left(\frac{\partial^2 U}{\partial X^2} + \frac{\partial^2 U}{\partial Y^2}\right) - \frac{Pr}{Da}(1+Nv\phi)u, \tag{27}$$

$$\begin{aligned}\varepsilon^{-2}\left(\frac{\rho_{nf}}{\rho_{bf}}\right)\left(U\frac{\partial V}{\partial X} + V\frac{\partial V}{\partial Y}\right) &= -\frac{\partial P}{\partial Y} + Pr\varepsilon^{-1}(1+Nv\phi)\left(\frac{\partial^2 V}{\partial X^2} + \frac{\partial^2 V}{\partial Y^2}\right)\\ &+ Ra{\cdot}Pr\left(\frac{\beta_{nf}}{\beta_{bf}}\right)\left(\frac{\rho_{nf}}{\rho_{bf}}\right)\theta_{nf} - \frac{Pr}{Da}(1+Nv\phi)v,\end{aligned} \tag{28}$$

$$Cr\left(U\frac{\partial \theta_{nf}}{\partial X} + V\frac{\partial \theta_{nf}}{\partial Y}\right) = \varepsilon(1+Nc\phi)\left(\frac{\partial^2 \theta_{nf}}{\partial X^2} + \frac{\partial^2 \theta_{nf}}{\partial Y^2}\right) + H\left(\theta_s - \theta_{nf}\right), \tag{29}$$

$$0 = K_r(1-\varepsilon)\left(\frac{\partial^2 \theta_s}{\partial X^2} + \frac{\partial^2 \theta_s}{\partial Y^2}\right) - H\left(\theta_s - \theta_{nf}\right). \tag{30}$$

3. Thick wall:

$$R_k\left(\frac{\partial^2 \theta_w}{\partial X^2} + \frac{\partial^2 \theta_w}{\partial Y^2}\right) = 0, \tag{31}$$

where

$$Ra=\frac{g\rho_{bf}\beta_{bf}\Delta TL^3}{\alpha_{bf}\mu_{bf}},Pr=\frac{\mu_{bf}}{\rho_{bf}\alpha_{bf}},Da=\frac{K}{L^2},H=\frac{hL^2}{k_{bf}},R_k=\frac{k_w}{k_{bf}},K_r=\frac{k_s}{k_{bf}}$$
$$\left(\frac{\rho_{nf}}{\rho_{bf}}\right)=(1-\phi)+\phi\left(\frac{\rho_p}{\rho_{bf}}\right),\left(\frac{\beta_{nf}}{\beta_{bf}}\right)=(1-\phi)+\phi\left(\frac{\beta_p}{\beta_{bf}}\right). \tag{32}$$

The thermal expansion behavior of the base fluid and the NEPCM particles are assumed similar ($\beta_{nf}/\beta_{bf}\sim 1$). The heat capacity ratio is evaluated using:

$$Cr=\frac{(\rho C_p)_{nf}}{(\rho C_p)_{bf}}=(1-\phi)+\phi\lambda+\frac{\phi}{\delta Ste}f, \tag{33}$$

in which f is:

$$f=\frac{\pi}{2}\sin\left(\frac{\pi}{\delta}(\theta-\theta_{fu}+\delta/2)\right)\Xi$$
$$\Xi=\begin{cases}0 & \theta<\theta_{fu}-\delta/2\\ 1 & \theta_{fu}-\delta/2<\theta<\theta_{fu}+\delta/2\\ 0 & \theta>\theta_{fu}+\delta/2\end{cases}\Bigg|\ \theta_{fu}=\frac{T_{fu}-T_c}{\Delta T}, \tag{34}$$

and λ, δ, and Ste are, respectively,

$$\lambda=\frac{\rho_{co}\rho_{sh}(C_{p,co}+\iota C_{p,sh})}{(\rho C_p)_{bf}(\rho_{sh}+\iota\rho_{co})},\delta=\frac{T_{Mr}}{\Delta T},Ste=\frac{(\rho C_p)_{bf}\Delta T(\rho_{sh}+\iota\rho_{co})}{\alpha_{bf}(h_{sf}\rho_{co}\rho_{sh})}. \tag{35}$$

2.4 | Nondimensional forms of the boundary and interface conditions

Interface boundary of the clear and porous layers:

$$V_{CL}=V_{PL},U_{CL}=U_{PL},\left.\frac{\partial U}{\partial N}\right|_{CL}=\frac{1}{\varepsilon}\left.\frac{\partial U}{\partial N}\right|_{PL},\left.\frac{\partial V}{\partial N}\right|_{CL}=\frac{1}{\varepsilon}\left.\frac{\partial V}{\partial N}\right|_{PL},\theta_{nf}|_{CL}=\theta_{nf}|_{PL}=\theta_s|_{PL}$$
$$(1+Nc\phi)\left.\frac{\partial\theta_{nf}}{\partial N}\right|_{CL}=\varepsilon(1+Nc\phi)\left.\frac{\partial\theta_{nf}}{\partial N}\right|_{PL}+(1-\varepsilon)K_r\left.\frac{\partial\theta_s}{\partial N}\right|_{PL}=\frac{q_i''L}{k_{bf}\Delta T}=Q_i. \tag{36}$$

Interface boundary of the wall and porous layer:

$$\theta_w|_{wall}=\theta_{nf}|_{PL}=\theta_s|_{PL}$$
$$R_k\left.\frac{\partial\theta_w}{\partial N}\right|_{wall}=\varepsilon(1+Nc\phi)\left.\frac{\partial\theta_{nf}}{\partial N}\right|_{PL}+(1-\varepsilon)K_r\left.\frac{\partial\theta_s}{\partial N}\right|_{PL}=\frac{q_i''L}{k_{bf}\Delta T}=Q_i. \tag{37}$$

Boundary conditions on the outer surfaces:

$$\begin{aligned} &V(X,0)=U(X,0)=0, \quad \frac{\partial\theta_w(X,0)}{\partial Y}=\frac{\partial\theta_{nf}(X,0)}{\partial Y}=\frac{\partial\theta_s(X,0)}{\partial Y}=0\\ &V(X,1)=U(X,1)=0, \quad \frac{\partial\theta_w(X,1)}{\partial Y}=\frac{\partial\theta_{nf}(X,1)}{\partial Y}=\frac{\partial\theta_s(X,1)}{\partial Y}=0\\ &V(1,Y)=0, U(1,Y)=0, \quad \theta_w(0,Y)=1, \theta_{nf}(1,Y)=0. \end{aligned} \tag{38}$$

A reference pressure point at the top of wall-porous layer interface with zero pressure is introduced. The physical quantity of interest in the current study is the heat transfer through the wall Q_w:

$$Q_w=-R_k\left(\frac{\partial\theta_w}{\partial X}\right)_{X=0,D}. \tag{39}$$

In addition, the heat transfer rates through the fluid and solid structures of the porous medium are respectively defined as:

$$Nu_{nfp}=-(1+Nc\phi)\left(\frac{\partial\theta_{nf}}{\partial X}\right)_{X=D}, Nu_s=-K_r\left(\frac{\partial\theta_s}{\partial X}\right)_{X=D}. \tag{40}$$

The average rate of heat passing through the wall $\bar{Q_w}$, and the average Nusselt numbers $\bar{Nu_{nfp}}$, and $\bar{Nu_s}$ are

$$\bar{Q_w}=\int_0^1 Q_w dY, \quad \bar{Nu}=\int_0^1 Nu dY. \tag{41}$$

Moreover, by using Equation 37, the following relation at the interfaces of the wall-porous layer can be established as

$$\bar{Q_w}=\varepsilon\bar{Nu_{nfp}}+(1-\varepsilon)\bar{Nu_s} \text{ at } X=D. \tag{42}$$

To find the impact of dispersing the nano-encapsulated particles, the below-mentioned ratios can be discussed:

$$Q_r=\frac{\bar{Q_w}|_{\varphi}}{\bar{Q_w}|_{\varphi=0}}, Q_r^{'}=\frac{\bar{Q_w}|_{\varphi,Ste\to\infty}}{\bar{Q_w}|_{\varphi=0}}, Q_r^{''}=\frac{Q_r}{Q_r^{'}}=\frac{\bar{Q_w}|_{\varphi}}{\bar{Q_w}|_{\varphi,Ste\to\infty}}. \tag{43}$$

Q_r ratio shows the augmentation or reduction of the heat transfer rate because of dispersing the NEPCM particles inside the host fluid. When the core of the NEPCM particles does not undergo any phase change, the impacts of dispersing the particles inside the base fluid is represented by $Q_r^{'}$. On the other hand, when the core of the particles experiences phase change, the influence of the presence of the NEPCM on the total heat transfer is investigated by $Q_r^{''}$. Ultimately, a Poisson equation is solved to better visualize the suspension flow:

$$\frac{\partial^2\Psi}{\partial X^2}+\frac{\partial^2\Psi}{\partial Y^2}=-\left(\frac{\partial V}{\partial X}-\frac{\partial U}{\partial Y}\right). \tag{44}$$

The cavity walls are considered as $\Psi=0$.

3 | NUMERICAL METHOD AND VALIDATIONS

3.1 | Grid check and validations

The nondimensional governing equations subject to the boundary conditions is solved numerically using a weighted finite element method, named Galerkin method. The discretization of the computational region is done using a nonuniform structured grid. The damped Newton approach is applied to fully couple the governing discretized equations. Finally, the solution for the corresponding linear algebraic equations is acquired using the Parallel Sparse Direct Solver. The computation is terminated when the residuals for all dependent variables become less than 10^{-5}. The used numerical method is described in detail in Zienkiewicz et al.[54]

The grid check survey is conducted for the present study to guarantee a grid independent solution. Five various nonuniform grid sizes are considered to select the appropriate grid size, as tabulated in Table 2. The results for the average Nusselt number over the hot vertical wall and the maximum velocity inside the porous cavity are presented for each grid size when $Ste = 0.2$, $\theta_f = 0.1$, and $\phi = 0.05$. It is noteworthy that the grids generated near the vertical and horizontal boundaries are considered denser to handle the steep gradients of temperature and velocity. Consequently, by considering the computational cost and accuracy, the nonuniform grid size of 150×150, specified in bold in Table 2, has been selected for the following analysis.

3.2 | Validations with others

The accuracy of the utilized numerical code can be proved by comparisons between the current outcomes and those reported in other studies.[55–58] Tables 3 and 4 and Figure 2 show these evaluations. As seen, the utilized code is reliable with high accuracy.

4 | RESULTS AND DISCUSSION

To focus the investigation on the phase change aspects of the core of the NEPCMs particles, we varied the volume fraction of the NEPCM particles in the range of $0.0 \le \phi \le 5\%$, dimensionless fusion temperature in the range of $0.05 \le \theta_f \le 1$, and the Stefan number in the range of $0.2 \le Ste \le \infty$. While the other parameters are fixed at $Pr = 6.2$, $Nc = 23.8$, $Nv = 12.5$, $\delta = 0.05$, $Ra = 10^6$, $D = 0.15$, $S = 0.35$, $\varepsilon = 0.8$, $Da = 10^{-2}$, $H = 500$, $K_r = 10$, and $R_k = 50$, $\lambda = 0.32$. The present study is set as dimensionless; however, for brevity, the "nondimensional" is dropped from the parameters in the forthcoming discussions.

Figure 3 portrays the influence of the fusion temperature (θ_f) on the streamlines, isotherms, and melting-solidification zone. Since we set the study for dominant natural convection ($Ra = 10^6$), strong recirculation and

TABLE 2 Grid test when $Ste = 0.2$, $\theta_f = 0.1$, and $\phi = 5\%$

Number of elements	Q_w	*Error* (%)	Ψ_{max}	*Error* (%)
50×50	20.643		32.392	
100×100	20.646	0.0145	32.455	0.1945
150×150	**20.652**	**0.0290**	**32.465**	**0.0308**
200×200	20.653	0.0049	32.469	0.0123
250×250	20.653	0	32.471	0.0061

Note. Bold indicates the utilized grid size for computations.

TABLE 3 A comparison between the results of current work and those of Kahveci[55] for the average Nusselt number when $Ra = 10^6$

ϕ	**0**	**0.05**
Present study	9.20	9.76
Kahveci et al[44]	9.23	9.783

TABLE 4 The average Nussle number of a porous media occupied with a suspension of water and Cu particles for $Ra \times Da = 10^3$

ϕ	Sheremet et al[57]	Sun and Pop[56]	Present work
0.1	9.41	9.42	9.42
0.2	12.84	12.85	12.85

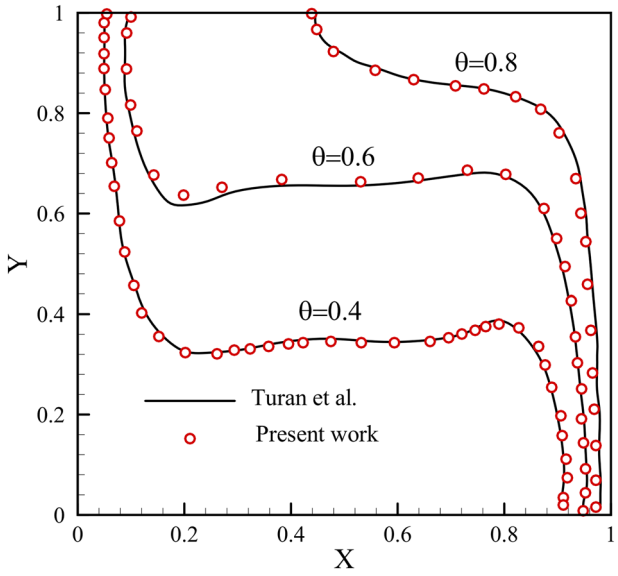

FIGURE 2 Temperature distribution obtained in the current code and by Turan et al[58] [Colour figure can be viewed at wileyonlinelibrary.com]

stratified isotherms are observed in the first and second columns of Figure 3, respectively. With very low fusion temperate ($\theta_f = 0.1$), Figure 3A depicts a strong recirculation, and the distribution of the heat capacity ratio, that is, *Cr*, (the fourth column) shows that the phase change process of the core of the NEPCM particles undergoes within a limited zone (melting-solidification zone). In fact, the core of the NEPCM particles on the left side of the melting-solidification zone is fully melted, and it release the stored heat while passing through this zone. Increasing θ_f from 0.1 to 0.4, the zone of the phase change expands and moves away from the cold wall and tends toward the center of the enclosure. As

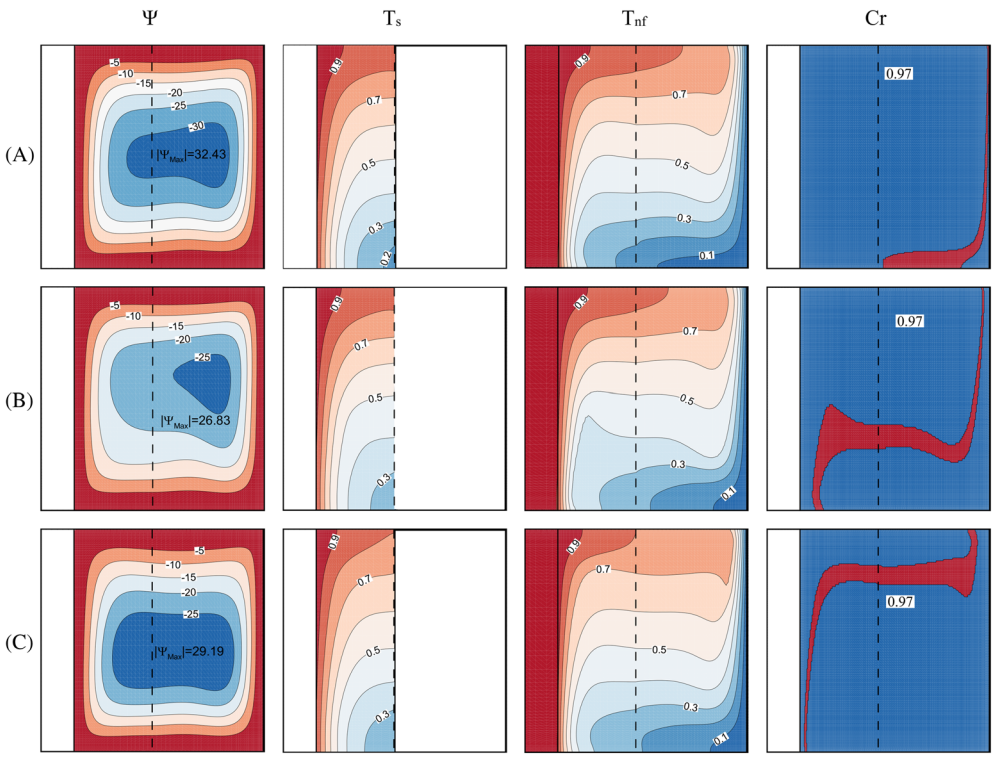

FIGURE 3 Streamlines, isotherms, and heat capacity ratio contours with fusion temperature: (A) $\theta_f = 0.1$, (B) $\theta_f = 0.4$, (C) and $\theta_f = 0.7$ when $Ste = 0.2$ and $\phi = 5\%$ [Colour figure can be viewed at wileyonlinelibrary.com]

a result, more NEPCM particles can undergo the phase change. The flow paths demonstrate that when $\theta_f = 0.4$, a large number of NEPCM particles passes through the melting-solidification zone. This, in turn, emerges higher thermal storage by the NEPCM particles; thus, the recirculation weakens, as shown in Figure 3B. For higher fusion temperature ($\theta_f = 0.7$), the melting-solidification zone becomes close to the solid wall and fewer NEPCM particles undergo the phase change; thus, the recirculation recovers some strength and expands to the porous layer (Figure 3C). It must be asserted that the isotherms of the fluid phase corresponding to the fusion temperature, shown in the third column of Figure 3, are most affected by the fusion temperature value. In fact, it is obvious that the surface of isothermal area surrounding the melting point temperature is expanded. The reason is that the heat is more absorbed by the core of nanoparticles during the phase change process with approximately no temperature rise. The temperature field of the fluid phase perceptibly is similar to that of the solid matrix in the areas far from the solidification-melting zones (the second column). However, it is found that the phase change of the core of the NEPCM particles amplifies the LTNE between the suspension and the solid matrix.

To investigate the effect of the Stefan number (*Ste*), the scenario of Figure 3 is repeated for a higher *Ste* of 0.7, and the results are presented in Figure 4. High *Ste* accounts for low latent heat of the NEPCM particles. Therefore, the phase change zones shrink, and the NEPCM particles absorb less heat energy compared with those of $Ste = 0.2$. Consequently, the stored heat in the core of the NEPCMs particles decreases, and this results in magnifying the stream function, as shown in Figure 4. Finally, it can be seen that the dependency of the governing fields on the θ_f increases when the *Ste* decreases.

For $\theta_f = 0.4$ and $Ste = 0.2$, the effect of the volume fraction of the NEPCM particles, that is, ϕ, on the governing fields is considered and presented in Figure 5. As Figure 5A to C illustrates, dispersing more NEPCMs inside the host fluid elevates the flow strength. The second column of Figure 4 shows that the isotherms of the solid matrix move slightly toward to the side solid wall and the upper bound of the enclosure. This trend can also be seen for the temperature field of the fluid phase, leading to an increase in the temperature gradient. The fluid temperature remains approximately constant in a wider area with the increment of the volume fraction of NEPCMs. This can be manifestly seen from the movement of the isotherms in the vicinity of the corresponding fusion temperature, resulting in a larger area with constant temperature. This is due to the core of a larger number of NEPCMs undergoes the phase change. Thus, the heat is stored in the core of NEPCM particles during phase change, resulting in an increase in the surface of the isothermal area.

The maps presented in Figure 6 display the variations of the average heat transfer in the cavity. The figure shows that the NEPCM particles dispersed in the host fluid augment the heat transfer in the cavity; this is due to the

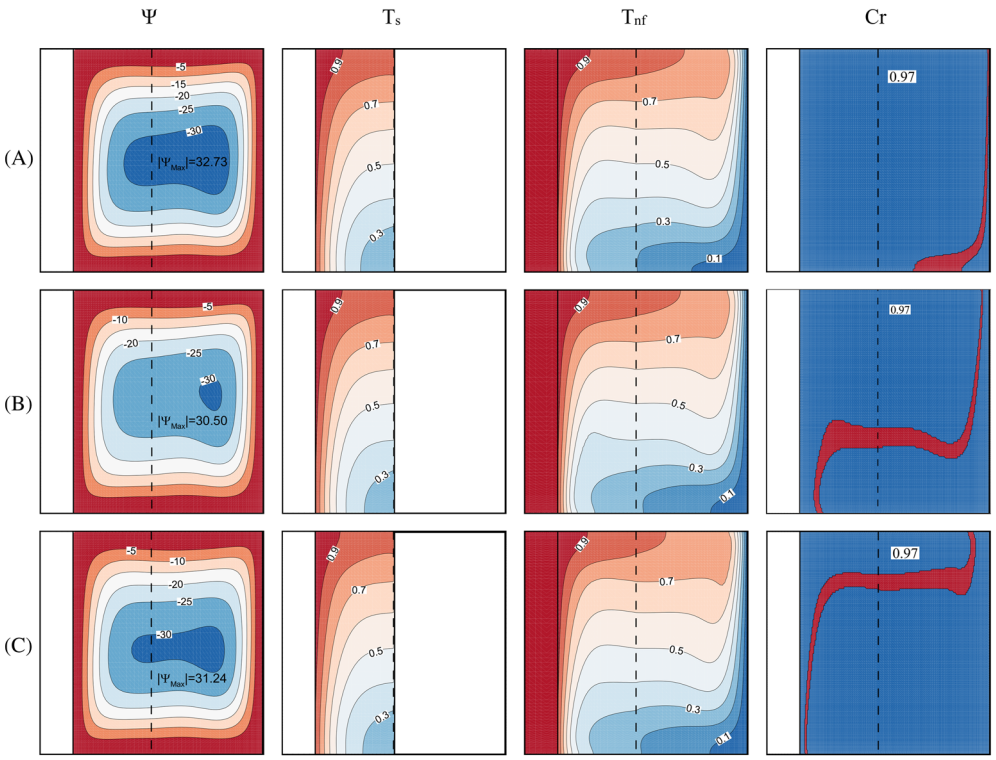

FIGURE 4 Streamlines, isotherms, and heat capacity ratio contours with fusion temperature: (A) $\theta_f = 0.1$, (B) $\theta_f = 0.4$, and (C) $\theta_f = 0.7$ when $Ste = 0.7$ and $\phi = 5\%$ [Colour figure can be viewed at wileyonlinelibrary.com]

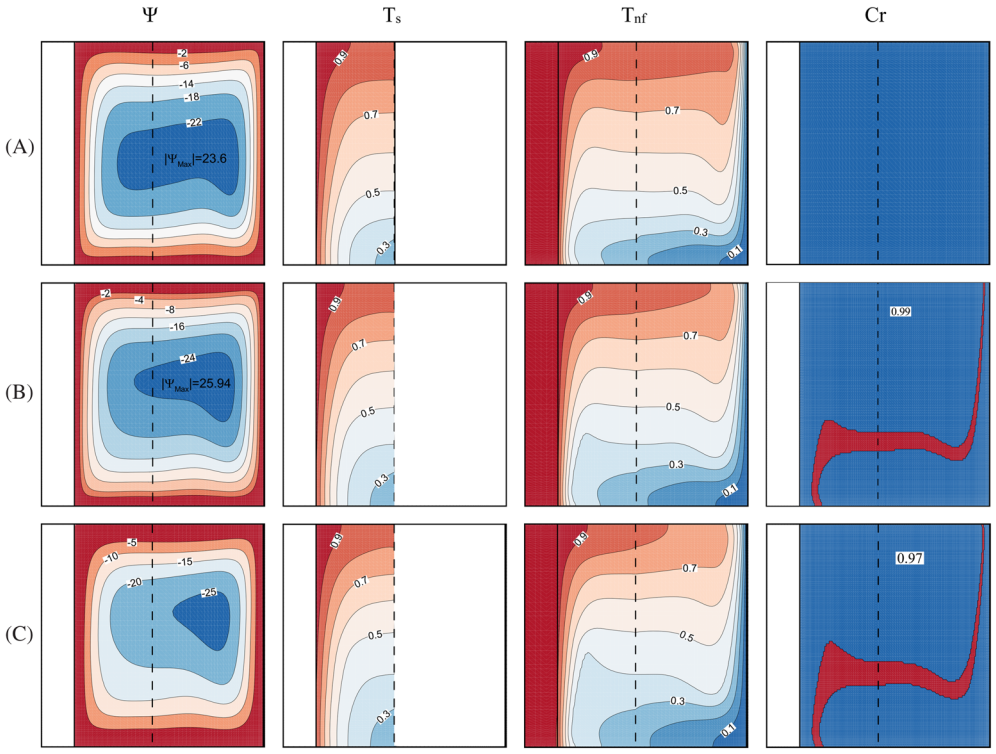

FIGURE 5 Streamlines, isotherms, and Cr ratio contours with volume fraction of the NEPCMs particles: (A) $\phi = 0.0$, (B) $\phi = 0.025$, and (C) $\phi = 0.05$ when $Ste = 0.2$ and $\theta_f = 0.4$ [Colour figure can be viewed at wileyonlinelibrary.com]

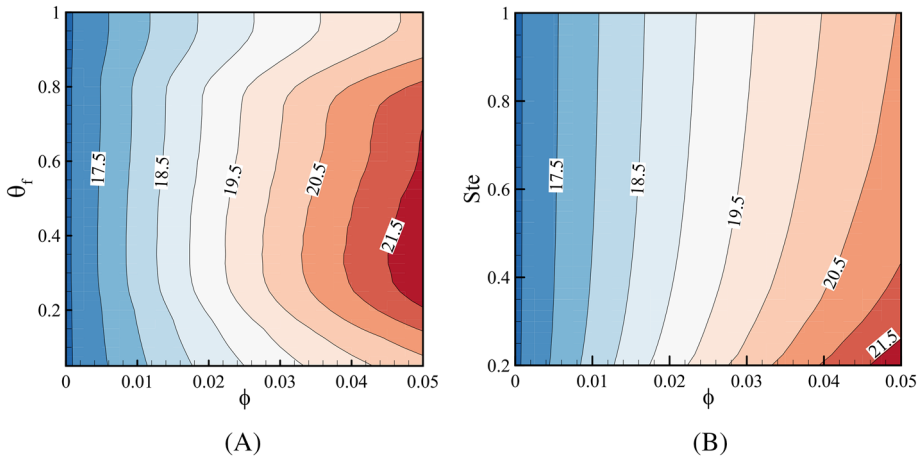

FIGURE 6 Maps of the average heat transfer $\bar{Q}_w$ for (A) θ_f and ϕ when $Ste = 0.2$ and (B) Ste and ϕ when $\theta_f = 0.4$ [Colour figure can be viewed at wileyonlinelibrary.com]

simultaneous increment of the thermal conductivity and heat capacity. Figure 6A indicates a marginal effect of fusion temperature on the heat transfer when $\phi \leq 0.01$. However, the bell-shaped lines of the constant heat transfer are associated when $\phi \geq 0.01$.

It is clear from Figure 6A that the maximum heat transfer occurs at the highest volume fraction and θ_f ranges from 0.2 to 0.6. This is due to that the maximum number of NEPCM particles undergo the phase change in this range of θ_f, due to the position of the melting-solidification zone. Essentially, when $0.2 \leq \theta_f \leq 0.4$, a larger number of NEPCM particles release their latent heat while passing the solidification-melting range (as depicted in Figures 3 and 4B). Hence, higher amount of heat can be transferred from the hot zone (the left side of the melting-solidification zone) to the cold one (the right side of the melting-solidification zone). The other map (Figure 6B) portrays an adverse effect of the Stefan number, especially at higher volume fraction. Stefan number inversely correlates with the latent heat of fusion, and hence, the higher *Ste*, the lower latent heat of fusion. Indeed, the higher values of *Ste* results in a reduction of the heat required for charging or fusion. This, as shown in Figure 6B, leads to a strong shrinkage in the range of the maximal heat transfer.

For a better understanding of dispersing the NEPCM particles in the base fluid, the ratio of the enhanced heat transfer to that of the pure fluid (Q_r) is plotted versus θ_f and *Ste* separately in Figure 7. According to Equation 33, neither θ_f

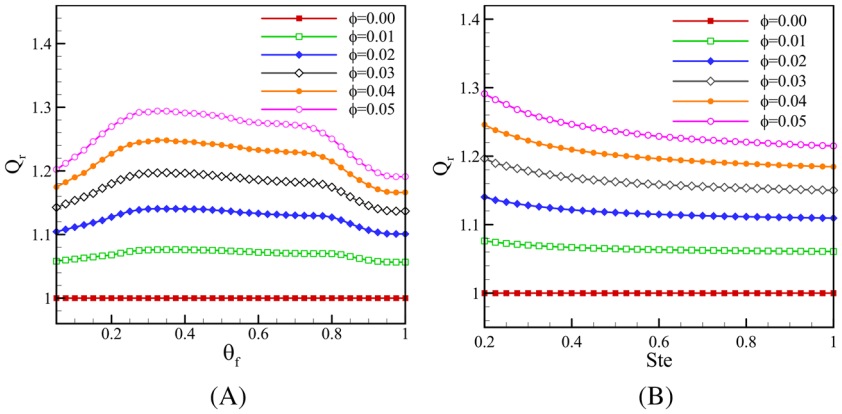

FIGURE 7 Variation of Q_r with (A) θ_f ($Ste = 0.2$) and (B) Ste ($\theta_f = 0.4$) for different values of volume fractions [Colour figure can be viewed at wileyonlinelibrary.com]

nor Ste affects the rate of heat transfer for pure fluid as no phase change undergoes. Figure 7A shows that the suspension composed of volume fraction of $\phi = 0.05$ and $\theta_f = 0.35$ enhances the heat transfer rate by 1.29 times compared with the pure fluid. Figure 7B presents that the adverse action of Ste is notably observed with the higher nanoparticles loading. Raising ϕ from 0 to 0.05, enhances Q_r by 29% and 22% when $Ste = 0.2$ and 1, respectively. Figure 8 displays the role of the NEPCM particles on the average heat transfer (shown with Q'_r), when their latent heat is negligible ($Ste \longrightarrow \infty$). The ratio of Q'_r that is given in Equation 43 shows that when Ste tends to ∞, the latent energy storage/release of nanoparticles approaches zero, and hence, the results of Figure 8 are independent of a fusion temperature. The figure endorses a continuous augmentation of the heat transfer rate with ϕ due to the enhancement of the thermal conductivity of the suspension.

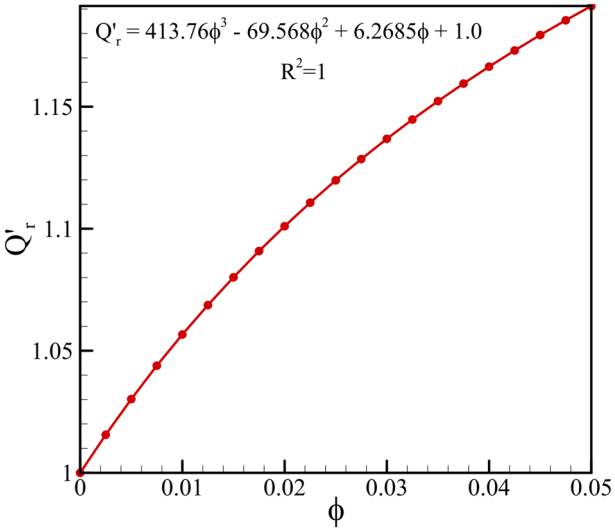

FIGURE 8 Variation of Q'_r with volume fraction of nano-encapsulated phase change materials (NEPCMs) [Colour figure can be viewed at wileyonlinelibrary.com]

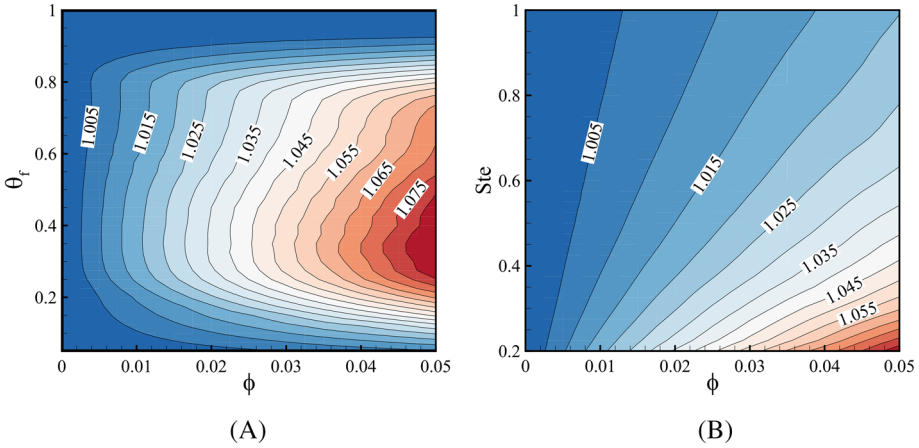

FIGURE 9 Variation of Q''_r with the volume fraction of nano-encapsulated phase change materials (NEPCMs) particles for (A) different values of fusion temperature ($Ste = 0.2$) and (B) Stefan number ($\theta_f = 0.4$) [Colour figure can be viewed at wileyonlinelibrary.com]

As shown by Q_r'' and mapped in Figure 9, the enhancement rate of the heat transfer induced by presence of the nano-capsules of PCMs is normalized with the case of simple nanoparticles with no phase change. The maps show a steep effect of fusion temperature even with moderate nanoparticles volume fraction. The perfect ranges that gives maximum rate of heat transfer are indicated when $\phi = 0.05$ and $0.25 \leq \theta_f \leq 0.475$, as shown in Figure 9A. Regarding Stefan number, Figure 9B asserts the adverse effect of lower latent heat of the core of the nanoparticles, and this effect becomes notable at high nanoparticles volume fraction.

5 | CONCLUSIONS

Three layers, solid, porous, and clear layer, confined in square cavity saturated with suspension of water and NEPCMs particles are heated differentially and analyzed numerically using the finite element method. The LTNE between the porous solid matrix and the suspension is taken into consideration. The study is focused on the effect of the fusion temperature of the core of NEPCM particles, Stefan number, and nanoparticles volume fraction. The numerical results were asserted to be accurate by comparing with other studies. The following conclusions are drawn from the results.

1. The LTNE is an important problem that should be taken into account with the analysis of heat transfer process of PCMs and especially when these materials are encapsulated in nanoparticles (NEPCM).
2. Higher Stefan number shrinks the zone of phase changing and deteriorates the rate of heat transfer in the overall system. This action of Stefan number becomes notable at higher volume fraction of NEPCMs.
3. Higher fusion temperature leads to rise up the melting phase change zone to the upper part of the cavity.
4. To get maximal heat transfer rate, the nanoparticles volume fraction should be as high as possible, and the fusion temperature should range between 0.2 and 0.6.
5. The enhancement of heat transfer rate can reach to about 29% when the volume fraction of the NEPCM is raised from 0 to 0.05.

CONFLICT OF INTEREST

This work does not have any conflicts of interest.

NOMENCLATURE

C_p specific heat capacity (J kg^{-1} K^{-1})
Cr heat capacity ratio
d thickness of the conjugate wall (m)
D nondimensional thickness of the conjugate wall
Da Darcy number
f nondimensional fusion function
g gravity (m s^{-2})
h the heat transfer coefficient between the suspension in pores and porous matrix (W m^{-3} K^{-1})
h_{sf} latent heat of the core (kJ kg^{-1})
H interface heat transfer coefficient
k thermal conductivity (W m^{-1} K^{-1})
K permeability of the porous medium (m^2)
K_r thermal conductivity ratio of the base fluid to the porous medium
L the length and width of size of the square cavity (m)
Nc number of thermal conductivity
Nv number of dynamic viscosity
$_{Nu}$ Nusselt number (local)
$\bar{Nu}$ Nusselt number (average)
p the suspension pressure (Pa)
P the nondimensional pressure of the suspension
Pr Prandtl number
q_i'' the total heat flux at interfacial interface (W m^{-2})
Q_w the nondimensional heat transfer at the conjugate wall (local)

$\bar{Q}_w$ the nondimensional heat transfer at the conjugate wall (average)
Ra Rayleigh number
R_k the ratio of the thermal conductivity of the wall to the thermal conductivity of the base fluid
s the thickness of the porous layer (m)
S nondimensional thickness of the porous layer
Ste Stefan number
T Temperature field (K)
T_{Mr} the phase change bond (K)
u, v velocity components along x, y directions, respectively (m s^{-1})
U, V dimensionless velocity components along X, Y directions, respectively
x, y Cartesian coordinates (m)
X, Y dimensionless Cartesian coordinates

GREEK SYMBOLS

α effective thermal diffusivity (m^2 s^{-1})
β the thermal expansion coefficient of the fluid (K^{-1})
δ nondimensional melting range
λ the sensible heat capacity ratio
ε porosity of the porous medium
θ dimensionless temperature
ι core-shell weight ratio
μ dynamic viscosity (kg m^{-1} s^{-1})
ρ density (kg m^{-3})
ϕ nanoparticle volume fraction
Ψ dimensionless stream function

SUBSCRIPTS

bf base fluid
c cold
CL clear layer
co core
eff effective
f fusion
h hot
nf suspension
p nanoparticle
PL porous layer
s solid porous matrix
sh nano particle's shell
w wall

ORCID

Mohammad Ghalambaz https://orcid.org/0000-0003-0965-2358

REFERENCES

1. Kośny J. *PCM-enhanced building components: an application of phase change materials in building envelopes and internal structures*. Springer; 2015.
2. Alawadhi EM, Amon CH. PCM thermal control unit for portable electronic devices: experimental and numerical studies. *IEEE Trans Compon Packag Tech*. 2003;26(1):116-125.
3. Khodadadi JM, Hosseinizadeh SF. Nanoparticle-enhanced phase change materials (NEPCM) with great potential for improved thermal energy storage. *Int Comm Heat Mass Tran*. 2007;34(5):534-543.
4. Farid MM, Khudhair AM, Razack SAK, Al-Hallaj S. A review on phase change energy storage: materials and applications. *Energ Conver Manage*. 2004;45(9–10):1597-1615.

5. Alsabery AI, Gedik E, Chamkha AJ, Hashim I. Impacts of heated rotating inner cylinder and two-phase nanofluid model on entropy generation and mixed convection in a square cavity. *Heat Mass Tran*. 2020;56(1):321-338.
6. Dogonchi AS, Tayebi T, Chamkha AJ, Ganji DD. Natural convection analysis in a square enclosure with a wavy circular heater under magnetic field and nanoparticles. *J Therm Anal Calorim*. 2020;139(1):661-671.
7. Tayebi T, Chamkha AJ, Djezzar M. Natural convection of CNT-water nanofluid in an annular space between confocal elliptic cylinders with constant heat flux on inner wall. *Scientia Iranica*. 2019;26(5):2770-2783.
8. Menni Y, Chamkha AJ, Zidani C, Benyoucef B. Numerical analysis of heat and nanofluid mass transfer in a channel with detached and attached baffle plates Numerical analysis of heat and nanofluid mass transfer in a channel with detached and attached baffle plates, n.d.
9. Mehryan S, Izadpanahi E, Ghalambaz M, Chamkha A. Mixed convection flow caused by an oscillating cylinder in a square cavity filled with Cu–Al 2 O 3/water hybrid nanofluid. *J Therml Anal Calorim*. 2019;137:965-982.
10. Ghalambaz M, Doostani A, Izadpanahi E, Chamkha AJ. Conjugate natural convection flow of Ag–MgO/water hybrid nanofluid in a square cavity. *J Therml Anal Calorim*. 2019;139(3):2321-2336.
11. Sheremet MA, Revnic C, Pop I. Free convection in a porous wavy cavity filled with a nanofluid using Buongiorno's mathematical model with thermal dispersion effect. *Appl Math Comput*. 2017;299:1-15.
12. Revnic C, Abu-Nada E, Grosan T, Pop I. Natural convection in a rectangular cavity filled with nanofluids. *Int J Numer Meth Heat Fluid Flow*. 2018;28(6):1410-1432.
13. Menni Y, Chamkha AJ, Azzi A. Nanofluid transport in porous media: a review. Special Topics & Reviews in Porous Media. *Int J*. 2019;10(1):49-64.
14. Menni Y, Chamkha AJ, Azzi A. Nanofluid flow in complex geometries—a review. *J Nanofluid*. 2019;8(5):893-916.
15. Menni Y, Chamkha AJ, Lorenzini G, Kaid N, Ameur H, Bensafi M. Advances of nanofluids in solar collectors—a review of numerical studies advances of nanofluids in solar collectors—a review of numerical studies. *Math Model Eng Probl*. 2019;6(3):415-427.
16. Faden M, König-Haagen A, Höhlein S, Brüggemann D. An implicit algorithm for melting and settling of phase change material inside macrocapsules. *Int J Heat Mass Tran*. 2018;117:757-767.
17. Hosseinizadeh SF, Darzi AR, Tan FL. Numerical investigations of unconstrained melting of nano-enhanced phase change material (NEPCM) inside a spherical container. *Int J Therm Sci*. 2012;51:77-83.
18. Ghalambaz M, Doostani A, Chamkha AJ, Ismael MA. Melting of nanoparticles-enhanced phase-change materials in an enclosure: effect of hybrid nanoparticles. *Int J Mech Sci*. 2017;134:85-97.
19. Jourabian M, Farhadi M, Darzi AAR. Outward melting of ice enhanced by Cu nanoparticles inside cylindrical horizontal annulus: Lattice Boltzmann approach. *App Math Model*. 2013;37(20–21):8813-8825.
20. Kashani S, Ranjbar AA, Madani MM, Mastiani M, Jalaly H. Numerical study of solidification of a nano-enhanced phase change material (NEPCM) in a thermal storage system. *J Appl Mech Tech Phys*. 2013;54(5):702-712.
21. Elbahjaoui R, El Qarnia H. Transient behavior analysis of the melting of nanoparticle-enhanced phase change material inside a rectangular latent heat storage unit. *Appl Therm Eng*. 2017;112:720-738.
22. Weaver JA, Viskanta R. Melting of frozen, porous media contained in a horizontal or a vertical, cylindrical capsule. *Int J Heat Mass Trans*. 1986;29(12):1943-1951.
23. Beckermann C, Viskanta R. Natural convection solid/liquid phase change in porous media. *Int J Heat Mass Tran*. 1988;31(1):35-46.
24. Trelles JP, Dufly JJ. Numerical simulation of porous latent heat thermal energy storage for thermoelectric cooling. *Appl Therm Eng*. 2003;23(13):1647-1664.
25. Vafai K, Sozen M. Analysis of energy and momentum transport for fluid flow through a porous bed. *J Heat Transfer*. 1990;112(3):690-699.
26. Alsabery AI, Ismael MA, Chamkha AJ, Hashim I. Effect of nonhomogeneous nanofluid model on transient natural convection in a non-Darcy porous cavity containing an inner solid body. *Int Comm Heat Mass Tran*. 2020;110:104442.
27. Ghalambaz M, Sabour M, Pop I, Wen D. Free convection heat transfer of MgO-MWCNTs/EG hybrid nanofluid in a porous complex shaped cavity with MHD and thermal radiation effects. *Int J Numer Meth Heat Fluid Flow*. 2019;29(11):4349-4376.
28. Dogonchi AS, Seyyedi SM, Hashemi-Tilehnoee M, Chamkha AJ, Ganji DD. Investigation of natural convection of magnetic nanofluid in an enclosure with a porous medium considering Brownian motion. *Case Stud Therm Eng*. 2019;14:100502.
29. Hashemi-Tilehnoee M, Dogonchi A, Seyyedi SM, Chamkha AJ, Ganji D. Magnetohydrodynamic natural convection and entropy generation analyses inside a nanofluid-filled incinerator-shaped porous cavity with wavy heater block. *J Therml Anal Calorim*. 2020;1-13. https: doi.org/10.1007/s10973-019-09220-6
30. Kaviany M. *Principles of heat transfer in porous media*. n/a: Springer Science & Business Media; 2012.
31. Kuznetsov AV, Vafai K. Analytical comparison and criteria for heat and mass transfer models in metal hydride packed beds. *Int J Heat Mass Tran*. 1995;38(15):2873-2884.
32. Vafai K. An investigation of a latent heat storage porous bed and condensing flow through it. *J Heat Transfer*. 1990;112(4):1014-1022.
33. Sheremet MA, Pop I, Nazar R. Natural convection in a square cavity filled with a porous medium saturated with a nanofluid using the thermal nonequilibrium model with a Tiwari and Das nanofluid model. *Int J Mech Sci*. 2015;100:312-321.
34. Alsabery AI, Chamkha AJ, Saleh H, Hashim I, Chanane B. Effects of finite wall thickness and sinusoidal heating on convection in nanofluid-saturated local thermal non-equilibrium porous cavity. *Phys Stat Mech Appl*. 2017;470:20-38.

35. Chamkha AJ, Sazegar S, Jamesahar E, Ghalambaz M. Thermal non-equilibrium heat transfer modeling of hybrid nanofluids in a structure composed of the layers of solid and porous media and free nanofluids. *Energies*. 2019;12(3):541.
36. Ghalambaz M, Tahmasebi A, Chamkha AJ, Wen D. Conjugate local thermal non-equilibrium heat transfer in a cavity filled with a porous medium: analysis of the element location. *Int J Heat Mass Trans*. 2019;138:941-960.
37. Harris KT, Haji-Sheikh A, Nnanna AA. Phase-change phenomena in porous media–a non-local thermal equilibrium model. *Int J Heat Mass Tran*. 2001;44(8):1619-1625.
38. Alsabery AI, Mohebbi R, Chamkha AJ, Hashim I. Effect of local thermal non-equilibrium model on natural convection in a nanofluid-filled wavy-walled porous cavity containing inner solid cylinder. *Chem Eng Sci*. 2019;201:247-263.
39. Ghalambaz M, Chamkha AJ, Wen D. Natural convective flow and heat transfer of nano-encapsulated phase change materials (NEPCMs) in a cavity. *Int J Heat Mass Tran*. 2019;138:738-749.
40. Hajjar A, Mehryan S, Ghalambaz M. Time periodic natural convection heat transfer in a nano-encapsulated phase-change suspension. *Int J Mech Sci*. 2019;166:105243.
41. Ghalambaz M, Groşan T, Pop I. Mixed convection boundary layer flow and heat transfer over a vertical plate embedded in a porous medium filled with a suspension of nano-encapsulated phase change materials. *J Mol Liq*. 2019;293:111432.
42. Ghalambaz M, Mehryan SAM, Hajjar A, Veismoradi A. Unsteady natural convection flow of a suspension comprising nano-encapsulated phase change materials (NEPCMs) in a porous medium. *Adv Powder Tech*. 2019. https://doi.org/10.1016/j.apt.2019.12.010
43. Alazmi B, Vafai K. Analysis of fluid flow and heat transfer interfacial conditions between a porous medium and a fluid layer. *Int J Heat Mass Tran*. 2001;44(9):1735-1749.
44. Vafai K, Thiyagaraja R. Analysis of flow and heat transfer at the interface region of a porous medium. *Int J Heat Mass Tran*. 1987;30(7):1391-1405.
45. Ochoa-Tapia JA, Whitaker S. Momentum transfer at the boundary between a porous medium and a homogeneous fluid—I. Theoretical development. *Int J Heat Mass Trans*. 1995;38(14):2635-2646.
46. Vafai K, Kim SJ. On the limitations of the Brinkman-Forchheimer-extended Darcy equation. *Int J Heat Fluid Flow*. 1995;16(1):11-15.
47. Betchen L, Straatman AG, Thompson BE. A nonequilibrium finite-volume model for conjugate fluid/porous/solid domains. *Numer Heat Trans, Part A: Appl*. 2006;49(6):543-565.
48. Chai L, Shaukat R, Wang L, Wang HS. A review on heat transfer and hydrodynamic characteristics of nano/microencapsulated phase change slurry (N/MPCS) in mini/microchannel heat sinks. *Appl Therm Eng*. 2018;135:334-349.
49. Chen B, Wang X, Zeng R, et al. An experimental study of convective heat transfer with microencapsulated phase change material suspension: laminar flow in a circular tube under constant heat flux. *Exp Therm Fluid Sci*. 2008;32(8):1638-1646.
50. Khanafer K, Vafai K. A critical synthesis of thermophysical characteristics of nanofluids. *Int J Heat Mass Tran*. 2011;54(19–20):4410-4428.
51. Seyf HR, Zhou Z, Ma HB, Zhang Y. Three dimensional numerical study of heat-transfer enhancement by nano-encapsulated phase change material slurry in microtube heat sinks with tangential impingement. *Int J Heat Mass Tran*. 2013;56(1–2):561-573.
52. Zaraki A, Ghalambaz M, Chamkha AJ, Ghalambaz M, De Rossi D. Theoretical analysis of natural convection boundary layer heat and mass transfer of nanofluids: effects of size, shape and type of nanoparticles, type of base fluid and working temperature. *Adv Powder Tech*. 2015;26(3):935-946.
53. Ghalambaz M, Doostani A, Izadpanahi E, Chamkha AJ. Phase-change heat transfer in a cavity heated from below: the effect of utilizing single or hybrid nanoparticles as additives. *J Taiwan Inst Chem Eng*. 2017;72:104-115.
54. Zienkiewicz OC, Taylor RL, Nithiarasu P, eds. *The Finite Element Method for Fluid Dynamics*. (Seventh Edition) ed. Oxford: Butterworth-Heinemann; 2014:iii.
55. Kahveci K. Buoyancy driven heat transfer of nanofluids in a tilted enclosure. *J Heat Transfer*. 2010;132(6):062501.
56. Sun Q, Pop I. Free convection in a triangle cavity filled with a porous medium saturated with nanofluids with flush mounted heater on the wall. *Int J Therm Sci*. 2011;50(11):2141-2153.
57. Sheremet MA, Grosan T, Pop I. Free convection in a square cavity filled with a porous medium saturated by nanofluid using Tiwari and Das' nanofluid model. *Transport Porous Media*. 2015;106(3):595-610.
58. Turan O, Sachdeva A, Chakraborty N, Poole RJ. Laminar natural convection of power-law fluids in a square enclosure with differentially heated side walls subjected to constant temperatures. *J Non-Newton Fluid Mech*. 2011;166(17):1049-1063.
59. Barlak S, Sara ON, Karaipekli A, Yapıcı S. Thermal conductivity and viscosity of nanofluids having nanoencapsulated phase change material. *Nanos Microsc Therm Eng*. 2016;20(2):85-96.
60. Ghalambaz M, Sheremet MA, Pop I. Free convection in a parallelogrammic porous cavity filled with a nanofluid using Tiwari and Das' nanofluid model. *PLoS ONE*. 2015;10(5):e0126486.

How to cite this article: Mehryan SAM, Ismael M, Ghalambaz M. Local thermal nonequilibrium conjugate natural convection of nano-encapsulated phase change particles in a partially porous enclosure. *Math Meth Appl Sci*. 2020;1–18. https://doi.org/10.1002/mma.6338